International Journal of Solids and Structures 50 (2013) 2224–2230

Contents lists available at SciVerse ScienceDirect

International Journal of Solids and Structures

journal homepage: www.elsevier.com/locate/ijsolstr

Phenomenological constitutive model for a CNT turf

H. Radhakrishnan, S.Dj. Mesarovic *, A. Qiu, D.F. Bahr

School of Mechanical and Materials Engineering, Washington State University, Pullman, WA 99164, USA

ARTICLE INFO

Article history:
Received 6 March 2012
Received in revised form 5 March 2013
Available online 11 April 2013

Keywords:
Carbon nanotubes
Collective behavior
Constitutive modeling
Finite elements
Nanoindentation
Viscoelasticity

ABSTRACT

Carbon nanotubes (CNT), grown on a substrate, form a *turf* – a complex structure of intertwined, mostly nominally vertical tubes, cross-linked by adhesive contact and few bracing tubes. The turfs are compliant and good thermal and electrical conductors. In this paper, we consider the micromechanical analysis of the turf deformation reported earlier, and develop a phenomenological constitutive model of the turf. We benchmark the developed model using a finite element implementation and compare the model predictions to the results two different nanoindentation tests.

The model includes: nonlinear elastic deformation, small Kelvin–Voigt type relaxation, caused by the thermally activated sliding of contacts, and adhesive contact between the turf and the indenter. The pre-existing (locked-in) strain energy of bent nanotubes produces a high initial tangent modulus, followed by an order of magnitude decrease in the tangent modulus with increasing deformation. The strong adhesion between the turf and indenter tip is due to the van der Waals interactions.

The finite element simulations capture the results from the nanoindentation experiments, including the loading, unloading, viscoelastic relaxation during hold, and adhesive pull-off.

1. Introduction

Since their discovery (Ijima, 1992) the properties of individual carbon nanotubes (CNTs) have been studied extensively[1], and are now well understood. The collective behavior of CNTs arranged in complex structures[2], *turfs*, is of interest in practical applications, such as nanoscale sensors and thermal switches (Christensen et al., 2003; Xu and Fisher, 2006) or adhesive gecko tapes (Ge et al., 2007).

Turf is a complex network of intertwined CNTs (Fig. 1). Their microstructure is the result of the growth process from the substrate (McCarter et al., 2006), during which the interplay of elastic bending energy and adhesive energy produces a local energy minimum in the configurational space (Mesarovic et al., 2007).

Given the growth method, the following question arises: Is the CNT turf a *material*, describable by a standard mathematical apparatus of continuum mechanics with effective properties, or – is it a *structure*, in which case a continuum model is not relevant? Moreover, the uniform compression experiments[3] reveal a curious type of nonlocal behavior – collective reorientation and buckling of a layer. The curious aspect of this behavior is that the nonlocality occurs under uniform loading (Zbib et al., 2008), but not under non-uniform loading such as nanoindentation, as we have shown in previous experimental works[4]. It has been suggested (Cao et al., 2005; Hutchens et al., 2010) that such behavior is the result of either non-homogenous properties of a material, or a structure-like behavior, not describable by continuum mechanics.

Our group has recently reported new experimental results designed specifically to answer the above questions (Qiu et al., 2011a). The turf is indeed a material, with negligible variation in local mechanical properties. Moreover, our uniform compression experiments (Zbib et al., 2008) produced a critical buckling stress independent of the turf width, indicating that collective reorientation and buckling of the boundary layer is the result of boundary conditions and intrinsic length scale, probably associated with the CNT wavelengths in initial configuration[5].

In the present communication, we concentrate on the behavior under localized loading, specifically nanoindentation, where the turf behaves as simple continuum. It exhibits reversible viscoelastic behavior even at large strains (McCarter et al., 2006; Qiu et al., 2011a,b). The analysis is complicated by the strong adhesion between the turf and the indenter. We propose a phenomenological model of the CNT turf, based on earlier micromechanical analysis

* Corresponding author. Tel.: +1 5093326697.
E-mail address: mesarovic@mme.wsu.edu (S.Dj. Mesarovic).

[1] See, for example: Bernholtz et al. (2002) for mechanical properties; Kim et al. (2001) and McClain et al. (2007) for electrical properties; and Osman and Srivastava (2001) and Cola et al. (2007) for thermal properties.

[2] As opposed to simple geometries, such as brushes (Qi et al., 2003; Waters et al., 2004), or bundles (Liu et al., 2005).

[3] Cao et al. (2005), Zbib et al. (2008), Hutchens et al. (2010).

[4] McCarter et al. (2006), Mesarovic et al. (2007), Qiu et al. (2011a).

[5] Hutchens et al. (2011) recently proposed a strain-softening constitutive model, where the buckling wavelength is related to the size of the computational cell. Our meso-scale studies (Torabi et al., 2013) demonstrate the intrinsic length scale related to the initial average curvature of CNTs.

0020-7683/$ - see front matter © 2013 Elsevier Ltd. All rights reserved.
http://dx.doi.org/10.1016/j.ijsolstr.2013.03.025

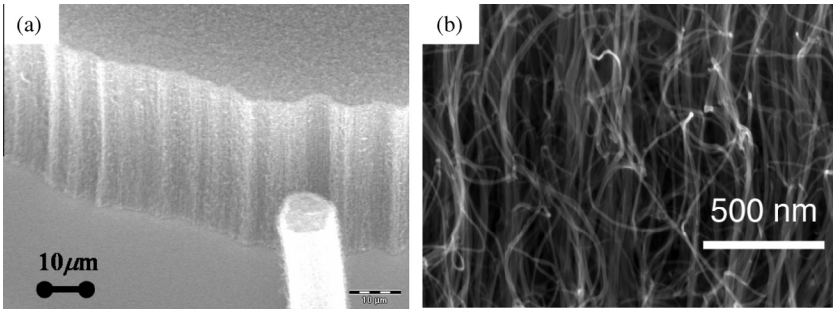

Fig. 1. SEM images of the carbon nanotube turf: (a) corner view, (b) detail.

(Mesarovic et al., 2007), and capable of reproducing the results from nanoindentation experiments. The turf is modeled as a nonlinear elastic continuum with viscous relaxation. An effective contact law is implemented to simulate the adhesion between the turf and the indenter.

The paper is organized as follows. In Section 2, we briefly describe the structure of the turf, experimental observations, and the micromechanical model. In Section 3, we describe the constitutive model of the turf. This is followed by the description of the finite element formulation in Section 4. The computational results and comparison between the model and experiments is presented in Section 5.

2. Structure and micromechanics of a CNT turf

As shown in Fig. 1(b), for most CNTs, their end-to-end line is close to vertical, but the segments are curved, and some have inclined or even horizontal end-to-end lines. The contacts between adjacent tubes are van der Waals bonded (Ajayan and Banhart, 2004). CNTs have high surface energy in air and low interface energy between in mutual contact, so the system tends to lower its energy through contact. Thus, the total energy of the assembly, E, is given as

$$E = U - \Gamma, \tag{1}$$

where U is the total elastic bending energy of CNTs, while Γ is the contact (adhesive) energy, defined as the difference between the total interface and surface energy of the assembly, and the surface energy of an imaginary contact-free assembly. As the configurational space is very large, many energy minima are expected. However, the experimentally observed mechanical reversibility (McCarter et al., 2006) indicates broad convex regions around the minima, so that – after moderate strains – the structure returns to its initial state. Nominally, the absolute energy minimum is achieved when the structure collapses laterally, i.e., with all tubes straight and in full contact (Liu et al., 2005). During initial stages of growth, the collapse is prevented by the substrate constraint. As the turf grows, the inclined and horizontal segments prevent the lateral collapse.

The earlier experiments (McCarter et al., 2006) using a Hysitron Triboscope with a blunt Berkovich tip, lead to the following conclusions (cf. Fig. 5):

(a) For moderately large strains the deformation is fully reversible.
(b) The turf exhibits time dependent relaxation. The mechanism suggested earlier (Mesarovic et al., 2007) is the thermally activated sliding and rearrangements of CNT contacts. Recent spring–mass models[6] indicate that dynamic events following local instabilities may be responsible for viscous dissipation.
(c) The load – indentation depth curve for the initial spherical portion of the indentation is almost linear, superficially similar to the behavior of an elastic – ideally plastic solid (Mesarovic and Fleck, 1999).
(d) The net tensile load required to pull-off the indenter from the turf during the retraction phase demonstrates adhesion of the turf with the indenter.

Mesarovic et al. (2007) have shown that the mechanism of deformation in the turf is easily understood by means of a simple micromechanical model of a free CNT segment with an initial curvature and contact patches at both the ends. Extended to the behavior of an assembly of such segments, the model implies a high initial tangent modulus followed by a rapid decrease in tangent modulus with increasing strain (hence the almost linear indentation loading curve). This prediction has been tested in the continuous stiffness indentation tests (Oliver and Pharr, 1992). The results, reported by McCarter et al. (2006), are consistent with the micromechanical model.

3. Constitutive model

The experimental measurements of the tangent modulus of CNT turfs (Fig. 2(a), McCarter et al., 2006) are consistent with the supercompressible foam behavior (Cao et al., 2005; Hutchens et al., 2010). The initially high tangent modulus drops by an order of magnitude with increasing strain. Using these observations, we represent the turf as isotropic compressible elastomeric hyperfoam material with a Kelvin–Voigt relaxation component. In the hyperfoam model (Storakers, 1986), the strain energy density U is expressed as the sum of non-integer powers of principal stretches, $\lambda_i (i = 1, 2, 3)$. For the sake of simplicity, we use only one term in the series:

$$U = \frac{2\mu_0}{\alpha^2}\left[\lambda_1^\alpha + \lambda_2^\alpha + \lambda_3^\alpha - 3 + \frac{(\lambda_1\lambda_2\lambda_3)^{\alpha\beta} - 1}{\beta}\right]. \tag{2}$$

Here, α and β are material parameters. The parameter β determines the degree of compressibility of the material and is related to the Poisson's ratio by

$$\nu = \frac{\beta}{1 + 2\beta}. \tag{3}$$

From (2) the nominal stresses, conjugate to the principal stretches can be expressed as

$$\sigma_j = \frac{1}{\lambda_j}\frac{2\mu_0}{\alpha}(\lambda_j^\alpha - J^{\alpha\beta}); \quad j = 1, 2, 3. \tag{4}$$

[6] Yang et al. (2011), Yang et al. (2012a,b), Fraternali et al. (2011), Blesgen et al. (2012).

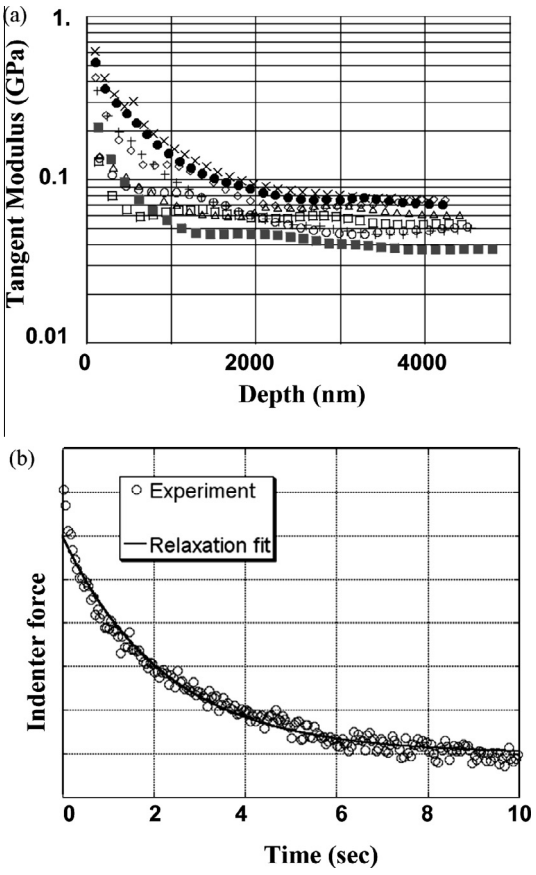

Fig. 2. (a) Tangent modulus of the turf as function of indentation depth using the continuous nanoindentation experiments measured at different locations on the CNT turf (Mesarovic et al., 2007). (b) Determination of the characteristic relaxation time of the turf using a curve fit between (8) and the experimental indenter force at constant indentation depth.

A ground-state (zero-stress state) is characterized by the initial shear μ_0 and the bulk modulus K_0:

$$K_0 = 2\mu_0\left(\beta + \frac{1}{3}\right). \tag{5}$$

Difficulties in measuring lateral deformation at nanoscale leave us without accurate value for the Poisson's ratio[7]. However, our computations indicate that the results are insensitive to this value. The results presented here are obtained with Poisson's ratio equal to zero, so that

$$\sigma_j = \frac{1}{\lambda_j}\frac{2\mu_0}{\alpha}(\lambda_j^{\alpha-1}). \tag{6}$$

The time dependent relaxation seen in the nanoindentation experiments is due to thermal sliding of contacts between the tubes. The time dependent relaxation is incorporated by assuming that the instantaneous shear modulus $\mu(t)$, varies as

$$\mu(t) = \mu_\infty + (\mu_0 - \mu_\infty)e^{-t/\tau}, \tag{7}$$

where μ_0 is the initial shear modulus, τ is the characteristic relaxation time, and μ_∞ is the relaxed shear modulus. Using the results from the controlled-depth indentation experiments, shown in Fig. 2(b), at constant indentation depth, the resultant load relaxes as

$$P(t) = P_\infty + (P_0 - P_\infty)e^{-t/\tau}, \tag{8}$$

[7] We are currently conducting computational studies using the meso-scale model, which are expected to give the value of the Poisson ratio.

where P_0 is the initial load and P_∞ is the load when $t \to \infty$. To obtain the relaxation time τ from experiments, we use the fit to the experimental force–time curve (Fig. 2(b)). The coefficients in (8) are obtained using the Newton–Raphson technique to minimize the error between (8) and the experimental curve.

The characteristic relaxation times during loading and unloading are the same: approximately 2.3 s. With the exception of the initial portion of the relaxation time (<0.25 s), a good agreement with the experimental relaxation curve can be obtained with a single term in the Kelvin–Voigt model (Fig. 2(b)). To complete the specification of the Kelvin–Voigt model, we specify the relative loss of shear modulus upon relaxation:

$$\bar{\mu} = \frac{\mu_0 - \mu_\infty}{\mu_0}. \tag{9}$$

By comparing the magnitude of relaxation in the FE results with the relaxation in constant load and constant depth portions of experiments, we estimate $\bar{\mu} \approx 0.35$.

4. Finite element model

We use the commercial finite element software ABAQUS (2006) and its user subroutine UNITER to define the interaction law between the turf and Berkovich nanoindenter. To obtain an economical 2D problem and retain the high accuracy of contact forces, we approximate the Berkovich three-sided pyramid with the equivalent conus, such that the cross-sectional areas of the Berkovich indenter and the rotationally symmetric conical indenter are the same at any distance from the apex of the indenter. This requires the conus with half-angle of 70.3°.

The FE analysis of the nanoindentation experiments on the CNT turf was performed using a rotationally symmetric mesh with linear triangular elements. A variable density mesh, shown in Fig. 3(a), was used. The dense mesh close to the contact was required to capture the surface tractions accurately. In additional to linear elements, we have performed test runs with the identical mesh of quadratic triangular elements, modified to support constant face pressure, to ensure accuracy and mesh convergence. To avoid the influence of outer boundary conditions, the size of the domain was greater than ten times the largest contact radius (Mesarovic and Fleck, 1999). The indenter tip was modeled as a rigid surface with the interactive forces between the turf and the indenter.

To ensure the validity of the model under different experimental conditions, we consider two different nanoindentation setups:

(a) The load-controlled experiment (Hysitron triboscope) with a blunt tip. The blunt section of the indenter is represented by a spherical section with a radius of curvature of 1.8 μm up to a depth of 150 nm. For numerical stability, the transition between the spherical and conical portions of the indenter is smoothed using a fillet with a large radius of curvature.
(b) The depth-controlled experiment (Hysitron triboindenter) with a sharp tip. The indenter with a sharp tip is modeled wholly with the equivalent conus.

The adhesive contact between the diamond Berkovich tip and the CNT turf is the result of van der Waals interactions. The interaction between CNT walls is usually modeled using the Lennard–Jones type force law (Zhao and Spain, 1989):

$$p(r) = \frac{9\gamma}{2r_0}\left[\left(\frac{r_0}{r}\right)^{10} - \left(\frac{r_0}{r}\right)^{4}\right], \tag{10}$$

where p is the contact pressure, γ is the surface energy, and r_0 is the equilibrium inter-atomic spacing (0.34 nm). However, the contact

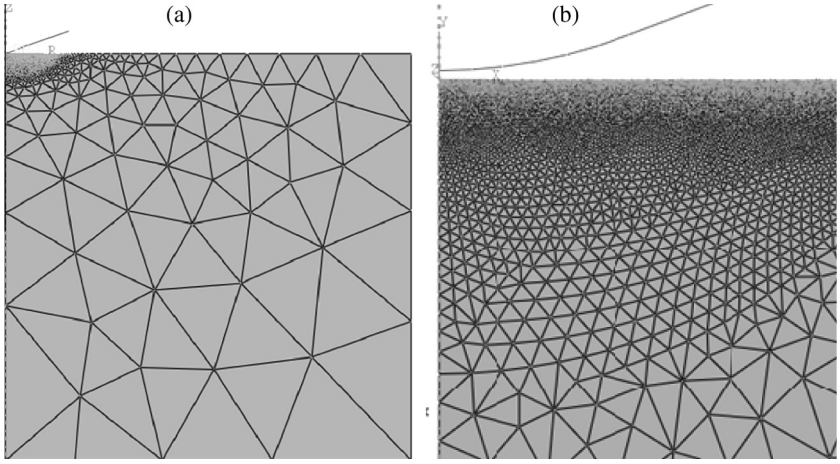

Fig. 3. (a) Axially symmetric finite element mesh with the Berkovich indenter tip represented as a rigid surface. (b) Detail of the mesh at the surface of the turf, showing the rounded tip of the blunt indenter.

law (10) is intended for interaction between static CNT walls and cannot be directly used for modeling the interacting between the turf and the indenter tip. The segments of CNTs at the surface are subject to thermal oscillations, resulting in an increased effective range of interactions. TEM observations by Treacy et al. (1996) on the vibration amplitude of CNTs as function of temperature confirm their thermal origin. The root mean square of the vibration amplitude of a CNT supported at one end was computed as

$$u^2 \approx 0.1061 kT\ell^3/EI, \tag{11}$$

where ℓ is the free standing length (7 μm), k is the Boltzmann constant, T is the absolute temperature, and EI is the bending stiffness of a nanotube. To calculate the bending stiffness of the multiwall nanotube we assume the elastic modulus as 0.4 TPa with tube inner and outer radii as 20 and 17.3 nm respectively.

Using (11), the displacement of a typical CNT at the surface of the turf is computed as 4.64 nm and this value is taken to represent the range of interactions, r_{int} (Fig. 4). The value r_{int} is derived as the abscissa intercept of the tangent to the zero curvature point. The modified force law (10) is flattened with a reduced maximum tensile traction but with the same surface energy as the original curve (Fig. 4). During the initial approach of the indenter, an unstable jump-to-contact occurs, as expected. The numerical solution for the unstable jump-to-contact and unstable pull-off requires either the arc-length algorithm, or a formulation which includes an artificial viscous damping term in addition to the contact tractions computed in (10). The viscous damping contact algorithm was thoroughly tested and is described in Radhakrishnan and Mesarovic (2009). The accuracy of the solution is ensured by checking that the ratio between the energy dissipated by viscous damping and the strain energy is always negligible (<0.01). A fine mesh with element size comparable to r_0 is required to accurately model the surface tractions between the indenter and the turf at the periphery of contact.

5. Results

To define the behavior of the turf, the values of the initial shear modulus μ_0, α and the relaxation properties τ and $\bar{\mu}$ are specified. From Fig. 2(a), it is observed that the initial tangent modulus of the turf varies between 0.6 and 0.2 GPa thereby giving an estimate of the initial shear modulus. In all the measurements, the ratio of the initial tangent modulus to the one at moderate strains is about 10. Suitable values of α are used in the FE analysis to ensure that this ratio is consistent with this observation. The appropriate

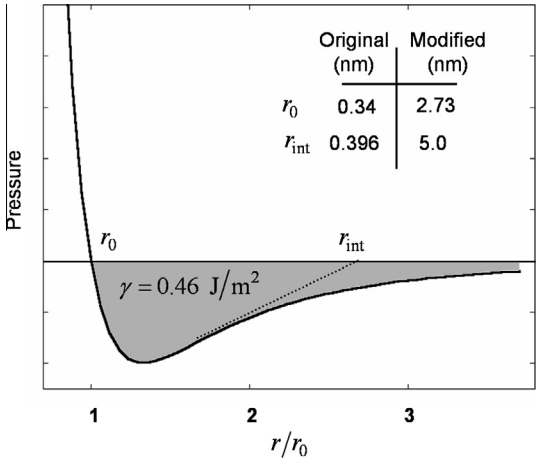

Fig. 4. Contact law used to model the van der Waals forces between the turf and the indenter. The original curve (10) is modified to include the effects of thermal vibrations of nanotubes.

values μ_0 and α are determined by fitting the FE results with the initial load-depth curves from experiments (segments **a-b** in Figs. 5 and 6(a)). The characteristic relaxation time τ is calculated in Fig. 2(b) as 2.3 s. The value of $\bar{\mu}$ is determined from the relaxation behavior of the turf by fitting the magnitude of relaxation from the FE results with the constant load and constant depth portions in experiments (segments **b-c** and **d-e** in Figs. 5 and 6(a)).

The loading mechanism of the Hysitron Triboscope is described McCarter et al. (2006) and its schematic is illustrated in Fig. 5(c), with Fig. 5(b) showing the loading history used in experiments. A Hysitron triboscope was used for the load-controlled experiments and the Hysitron Triboindenter for the depth-controlled experiments. The indenter mechanism in both cases was replicated in the finite element model using spring elements. Net repulsive forces between the indenter and the turf are shown as positive.

As in the experiments, we discard the initial jump-to-contact portion in the numerical results and the measurements start when there zero net force between the turf and the indenter. The best fit with experimental data was obtained with the initial shear modulus μ_0 = 230 MPa, and α = 18.8. The fit between computational and experimental results in Fig. 5(a) is satisfactory, including the

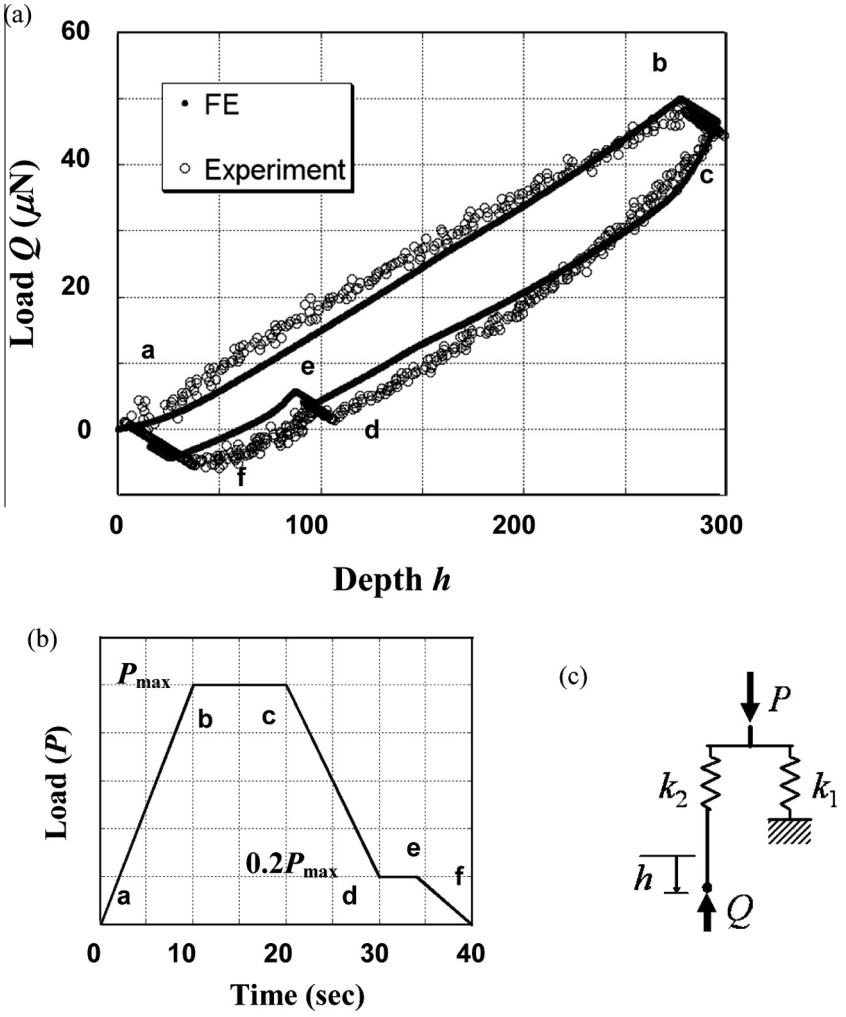

Fig. 5. (a) Comparison between FE results and load-controlled nanoindentation experiments (McCarter et al., 2006). (b) Loading history. (c) The loading mechanism of the Hysitron Triboscope. Note that the force P is controlled, not the actual contact force Q.

loading, viscoelastic relaxation, unloading and adhesive pull-off. The differences between the experiments and the model during unloading can be attributed to the differences between the equivalent cone and the blunt Berkovich indenter.

In the second experimental setup, a sharp Berkovich tip was used. The Hysitron Triboindenter utilizes a feedback loop to execute depth-controlled indentation regime. The values $\mu_0 = 50$ MPa and $\alpha = 9.1$ are determined by fitting the FE results to the experiments. The large difference between the properties of the samples produced in different batches is not surprising in view of the results shown in Fig. 2. It is also within the range of experimentally observed properties we reported earlier (Qiu et al., 2011a). In general, CNT turfs exhibit a great variability and the controlled manufacturing method is still an open problem.

The results shown in Fig. 6(a) indicate a satisfactory fit. A notable exception is the sharp change in the slope during computational unloading (point $\mathbf{c^1}$ in Fig. 6(a)). This "elbow" is the result of our neglecting the time-dependence of adhesion at the contact between the turf and indenter. The constant surface energy (10) leads to a constant contact area during the initial stages of unloading (segment $\mathbf{c\text{-}c^1}$ in Fig. 6(b)). The contact radius is defined by the maximum tensile traction. During the initial stages of unloading in regime $\mathbf{c\text{-}c^1}$, the contact radius remains constant but the size of the region under tensile tractions increases, leading to sharp drop in the indenter load (positive in compression). With further unloading, the turf begins to peel-off from the indenter and the start of the peel-off is seen as the sudden change in slope at $\mathbf{c^1}$ in Fig. 6(a). Recent experiments performed in our group (Qiu et al., 2011b) combine the nanoindentation with electrical conductivity measurements. The results indicate that while the nominal contact size remains constant in the early portions of the unloading, the length of tubes in contact decreases, thus gradually weakening the contact. The subsequent peel-off is therefore more gradual, so that the experimental load–displacement curve appears smooth, without sudden change in slope.

6. Summary and discussion

The nanoindentation experiments reveal that, under localized loading, CNT turfs exhibit highly compressible foam-like behavior with viscous relaxation as the result of thermally activated sliding of contacts. The deformation is shown to be fully mechanically reversible (viscoelastic) under moderate strains. The isotropic hyperfoam material model with a Kelvin–Voigt relaxation component serves as a first approximation.

The parameters in the hyperfoam model and the Kelvin–Voigt model are determined from experimental observations and by fitting the FE results with the nanoindentation experiments. The Berkovich indenter tip is modeled with an equivalent conical indenter and the interaction between the turf and indenter is represented using Lennard–Jones type of contact law. The contact law is modified to account for the increased range of the interactive forces due

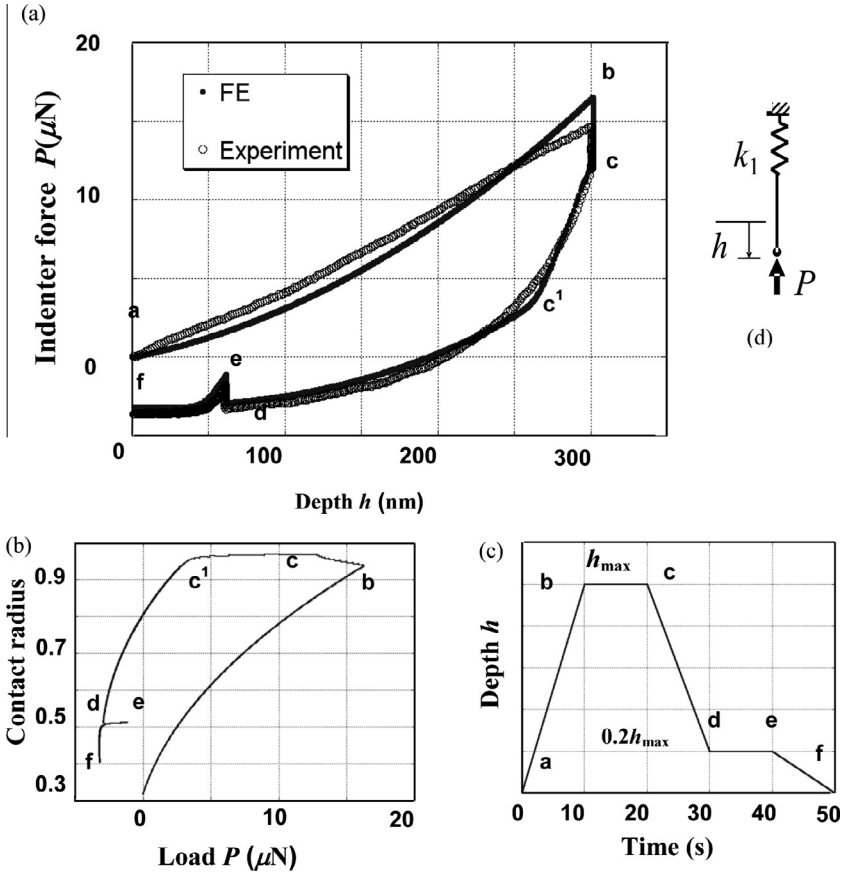

Fig. 6. (a) Comparison between FE results and depth-controlled nanoindentation experiments. (b) Contact radius as a function of indentation load. (c) Loading regime for depth-controlled experiments. (d) The loading mechanism of the Hysitron Triboindenter.

to thermal vibrations. The contact algorithm also includes negligible damping forces to resolve the unstable jump-to-contact and pull-off between the interacting surfaces.

We compare our computational results to two types on nanoindentation experiments: load-controlled nanoindentation with blunt (spherical cap) indenter, and depth-controlled nanoindentation with a sharp indenter. The finite element results demonstrate that a continuum model of the nanotube turf is capable of capturing the mechanical behavior under moderate strains seen in both the load-controlled and depth-controlled experiments. The minor differences during the unloading portion are the result of: (a) approximation of the Berkovich three-sided pyramid with cone, and, (b) the absence of contact creep in the FE model.

In contrast to nanoindentation results, CNT turfs exhibit irreversible reorientation of CNTs and collective buckling of a layer. While we do not consider that case in this paper, nano-scale simulations, intended to reveal the mechanisms and the intrinsic length scale associated with this behavior, are underway in our group. Nevertheless, the question of why such collective buckling does not occur under localized load can perhaps be answered at this time. Buckling of nanotubes will be irreversible only if it involves collective rearrangements of large number of segments, i.e., large volume. In contrast, buckling of a single segment with fixed ends (contacts) is expected to be fully reversible. Even if the ends (contacts) slide, they can slide back under reversed loading if the topology of the segments is not changed. Only the changes in topology (connectivity) are expected to yield mechanically irreversible behavior. Under localized loading, the segments in a small affected volume buckle, but the changes in topology are minimal or nonexistent, hence the mechanical reversibility.

Acknowledgments

This work has been supported by the US National Science Foundation, Grant # CTS-0856436. The authors are grateful to J. Jiao and D. McClain, Portland State University, for providing the initial turf samples.

References

ABAQUS, 2006. V6.7 User's manual. Hibbitt, Karlsson & Sorensen Inc., Pawtucket, R.I.

Ajayan, P.M., Banhart, F., 2004. Nanotubes: strong bundles. Nat. Mater. 3 (3), 135–136.

Bernholtz, J., Brenner, D., Buongiorno Nardelli, M., Meunier, V., Roland, C., 2002. Mechanical and electrical properties of nanotubes. Annu. Rev. Mater. Res. 32, 347–375.

Blesgen, T., Fraternali, F., Raney, J.R., Amendola, A., Daraio, C., 2012. Continuum limits of bistable spring models of carbon nanotube arrays accounting for material damage. Mech. Res. Commun. 45, 58–63.

Cao, A., Dickrell, P.L., Sawyer, W.G., Gahasemi-Nejhad, M.N., Ajayan, P.M., 2005. Super-compressible foamlike carbon nanotube films. Science 310 (5752), 1307–1310.

Christensen, A.O., Jacob, J.P., Richards, C.D., Bahr, D.F., Richards, R.F. 2003. Fabrication and characterization of a liquid–metal micro-droplet thermal switch. In: Proc. Transducers'03 Boston Paper No AM069.

Cola, B.A., Xu, J., Cheng, C., Xu, X., Fisher, T.S., 2007. Photoacoustic characterization of carbon nanotube array thermal interfaces. Appl. Phys. 101 (5), 054313–054321.

Fraternali, F., Blesgen, T., Amendola, A., Daraio, C., 2011. Multiscale mass–spring models of carbon nanotube foams. J. Mech. Phys. Solids 59, 89–102.

Ge, L., Sethi, S., Ci, L., Ajayan, P.M., Dhinojwala, A., 2007. Carbon nanotube-based synthetic gecko tapes. PNAS 104 (26), 10792–10795.

Hutchens, S.B., Hall, L.J., Greer, J.R., 2010. In situ mechanical testing reveals periodic buckle nucleation and propagation in carbon nanotube bundles. Adv. Funct. Mater. 20 (15), 2338–2346.

Hutchens, S.B., Needleman, A., Greer, J.R., 2011. Analysis of uniaxial compression of vertically aligned carbon nanotubes. J. Mech. Phys. Solids 59 (10), 2227–2237.

Ijima, S., 1992. Helical microtubules of graphitic carbon. Nature 354, 56–58.
Kim, P., Shi, L., Majumdar, A., McEuen, P.L., 2001. Thermal transport measurements of individual multiwalled nanotubes. Phys. Rev. Lett. 87 (21), 215502–215505.
Liu, J.Z., Zheng, Q.S., Wang, J.F., Jiang, Q., 2005. Mechanical properties of single-walled carbon nanotube bundles as bulk materials. J. Mech. Phys. Solids 53, 123–142.
McCarter, C.M., Richards, R.F., Mesarovic, S.Dj., Richards, C.D., Bahr, D.F., McClain, D., Jiao, J., 2006. Mechanical compliance of photolithographically defined vertically aligned carbon nanotube turf. J. Mater. Sci. 41 (23), 7872–7878.
McClain, D., Wu, J., Tavan, N., Jiao, J., McCarter, C.M., Richards, R.F., Mesarovic, S.Dj., Richards, C.D., Bahr, D.F., 2007. Electrostatic shielding in patterned carbon nanotube field emission arrays. Phys. Chem. C 111 (20), 7514–7520.
Mesarovic, S.Dj., Fleck, N.A., 1999. Spherical indentation of elastic–plastic solids. Proc. R. Soc. London A 455, 2707–2728.
Mesarovic, S.Dj., McCarter, C.M., Bahr, D.F., Radhakrishnan, H., Richards, R.F., Richards, C.D., McClain, D., Jiao, J., 2007. Mechanical behavior of a carbon nanotube turf. Scripta Mater. 56, 157–160.
Oliver, W.C., Pharr, G.M., 1992. An improved technique for determining hardness and elastic modulus using load and displacement sensing indentation experiments. J. Mater. Res. 7 (6), 1564–1583.
Osman, M.A., Srivastava, D., 2001. Temperature dependence of the thermal conductivity of single-wall carbon nanotubes. Nanotechnology 12 (1), 21–24.
Qi, H.J., Teo, K.B.K., Lau, K.K.S., Boyce, W.I., Milne, W.I., Robertson, J., Gleason, K.K., 2003. Determination of mechanical properties of carbon nanotubes and vertically aligned carbon nanotube forests using nanoindentation. J. Mech. Phys. Solids 51, 2213–2237.
Qiu, A., Bahr, D.F., Zbib, A.A., Bellou, A., Mesarovic, S.Dj., McClain, D., Hudson, W., Jiao, J., Kiener, D., Cordill, M.J., 2011a. Local and nonlocal behavior of CNT turfs and coordinated buckling of turf layers. Carbon 49 (4), 1430–1438.
Qiu, A., Fowler, S.P., Jiao, J., Kiener, D., Bahr, D.F., 2011b. Time-dependent contact behavior between diamond and a CNT turf. Nanotechnology 22 (29), 2957–2963.
Radhakrishnan, H., Mesarovic, S.Dj., 2009. Adhesive contact of elastic spheres revisited: numerical models and scaling. Proc. R. Soc. London A 465, 2231–2249.
Storakers, B., 1986. On material representation and constitutive branching in finite compressible elasticity. J. Mech. Phys. Solids 34 (2), 125–145.
Torabi, H., Radhakrishnan, H., Mesarovic, S. Dj., 2013. Micromechanics of collective buckling of carbon nanotubes. Manuscript in preparation.
Treacy, M.M.J., Ebbensen, T.W., Gibson, J.M., 1996. Exceptionally high Young's modulus observed for individual carbon nanotubes. Nature 381 (6584), 678–680.
Waters, J.F., Riester, L., Jouzi, M., Guduru, P.R., Xu, J.M., 2004. Buckling instabilities in multiwalled carbon nanotubes under uniaxial compression. Appl. Phys. Lett. 85 (10), 1787–1789.
Xu, J., Fisher, T.S., 2006. Enhancement of thermal interface materials with carbon nanotube arrays. Int. J. Heat Mass Transfer 49, 1658–1666.
Yang, X., He, P., Gao, H., 2012a. Competing elastic and adhesive interactions govern deformation behaviors of aligned carbon nanotube arrays. Appl. Phys. Lett. 101 (5), 053105.
Yang, X., He, P., Gao, H., 2012b. Modeling frequency- and temperature-invariant dissipative behaviors of randomly entangled carbon nanotube networks under cyclic loading. Nano Res. 4 (12), 1191–1198.
Zbib, A.A., Mesarovic, S.Dj., Lilleodden, E., McClain, D., Jiao, J., Bahr, D., 2008. Coordinated buckling of carbon nanotube turf under uniform compression. Nanotechnology 19 (17), 1757–1763.
Zhao, Y.X., Spain, I.L., 1989. X-ray diffraction data for graphite to 20 GPa. Phys. Rev. B 40 (2), 993–997.